RELIABILITY ANALYSIS OF A HYDRAULIC ON/OFF FAST SWITCHING VALVE

Niels C. Bender[1], Henrik C. Pedersen[1], Andreas Plöckinger[2] and Bernd Winkler[2]
[1]Department of Energy Technology. [2]Linz Center of Mechatronics GmbH
[1]Aalborg University. [2]Linz University, 4040 Linz, Austria
[1]Pontoppidanstraede 111, 9220 Aalborg, Denmark. [2]Altenbergstrasse 69
{ncb,hcp}@et.aau.dk, {Andreas.Ploeckinger,bernd.winkler}@lcm.at

ABSTRACT

This paper presents an analysis of a hydraulic on/off valve from a reliability point of view. The objective is to clarify the potential pitfalls of the current valve design, while identifying the component(s) exerting the most significant risk of failure during the lifetime of the valve. Specifically, the mechanical topology of Fast Switching hydraulic Valves (FSVs) are of interest since these undergo operating cycles in the gigacycle regime in theirs functional lifetime. Application of these FSVs is relevant in e.g. digital displacement units, which for the specific design considered, experience pressure differentials of 345 bar at flow rates of 120 L/min and impact velocities around 1 m/s. All of which introduce a concern about the severity of long term fatigue and wear. Answers to these concerns ire sought by first establishing a fault tree analysis of the FSV. Hereafter, the failure rates of different components are elaborated and expressions for such failure rates are established. This is done by a pseudo-analytic approach, where the expected reliability of the FSV is based upon statistical data. Results of two different cases are highlighted, namely failure with a low and high allowed internal leakage across the valve seat (0.0005 and 0.5 L/min). The study shows that the probability of a low leakage failure is close to 100% before 5 years of operation and 10% risk of high leakage failure after 25 years of operation. Valve seat failure is therefore a potential threat to limit the functional lifetime of the FSV. The applied reliability models involve a high amount of uncertainty, but there is a clear indication that failures will evolve around the flow passage. Allowing additional leakage prolongs the expected lifetime, and further work involves design of a framework to simulate design factors influencing the valves performance & lifetime.

KEYWORDS: Digital hydraulic valves, Failure mode analysis, Failure rate, Reliability

1 INTRODUCTION

The latest development in the field of fluid power technology towards increased efficiency is found in digital fluid power. This includes Digital Displacement (**DD**) machines, which have yielded theoretical part load efficiency superior to conventional hydraulic pumps and motors [1]. This technology is considered to be relevant as the key component in

hydrostatic transmission systems, potentially enhancing scalability. However, the lifetime of the system must not be compromised by this DD technology when compared with conventional mechanical transmission systems. Such a transmission system is of high relevance in e.g. wind turbines where exactly scalability and lifetime are important factors. Therefore, an analysis of the systems reliability is relevant.

DD machines rely on several Fast Switching Valves (**FSV**) in order to maintain the feasibility. Such FSVs are currently not commercially available, though several concepts have been proposed [2, 3, 4, 5, 6]. Most designs include performance demands imposing a concern about the durability of the FSVs. An experimental study of water hydraulic on/off poppet valves done by Paloniitty et al. [7] supports this concern showing significant wear after 1 million cycles. Applying virtual prototyping to limit this issue, without actual prototype testing, it is relevant to be able to simulate or estimate the durability of a given FSV design by describing the physical phenomena causing wear and fatigue.

With nearly 200 mechanical wear models identified in 1995 by Meng & Ludema [8], and more proposed since then, the prediction and modelling of mechanical wear is just not straight-forward as elaborated by Williams [9]. This paper is therefore solely focusing on statistics based models, and the aim is to extrapolate information from existing poppet valve data and apply it on the prototype FSV while discussing the approach and results.

This paper is structured as follows: Initially a presentation of the system of interest is given, thereafter a fault tree- & failure mode- analysis is presented to reveal the potential components where a failure or fault may occur. This analysis is extended to estimate the total failure rate of the system with help of some simplified models. The coefficients of these failure rates are visualized and the reliability is plotted against time. A discussion of the presented results are given aided by a structural analysis of the FSV. Finally the main conclusions are summed up.

2   PRESENTATION OF SYSTEM

The system analyzed in this paper is a FSV with focus on this component's application in a digital displacement machine. The prototype design of the FSV is shown in Fig. 1 [10]. The system comprise an actuator in the form of a copper coil moving in a magnetic field, a spring attached to the plunger to counteract flow forces, a flow geometry designed to deliver 120 l/min with a pressure difference around 0.5 bar and finally a housing assembly in which all the aforementioned components are contained.

The intended use of the FSV includes a passive opening caused by a pressure difference between corresponding inlet and outlet. While fluid is streaming through the seat, forces from the movement of fluid will exert a closing force on the plunger. When a current is running in the moving coil, a magnetic field will develop and due to the magnetic field from the permanent magnet a force will be exerted to close the valve. When closed, the plunger and seat are squeezed together to ensure that the flow passage is blocked and that no fluid can be transported from inlet to outlet. The functionality of the FSV is therefore compromised if either the actuator, spring or sealing feature of the valve fails.

The reliability of a system, e.g. of the one presented above, may be described by statistic and probabilistic models, where data of time until failure is used. A system is normally divided into three main phases; *'phase of infant mortality'* where the failure rate is high during a short amount of time (caused by product malformation or test uncertainties); *'useful lifetime phase'* which is characterised by a low failure rate and; *'wear out phase'* where the failure rate rises dramatically. These phases constitute the 'bathtub curve' [11]

Parameter	Value	Unit
Valve specs		
l_s	2.5	mm
$r_{i,1}, r_{o,1}, r_{i,2}, r_{o,2}$	11.5, 12.2, 17.6, 18.3	mm
D_c, D_w	14, 1.24	mm
v_0, v	2e-08, 8.1235e-08	lbfmin/in^2
p_1, p_2	5076.33, 72.519	psi
R_a	4	μin
Q_{f1}, Q_{f2}	0.03, 30	in^3/min
Q_r	31.7	gpm
Machine specs		
I_r	{0.2,0.4,0.6,0.8,1.0}	-
c_o, c_{10}	10, 10	μm
N_{10}	0.017	particle/h
Life expectancy	20-25	years
ω_{rated}	800	rpm
$T_{operating}$	60	℃
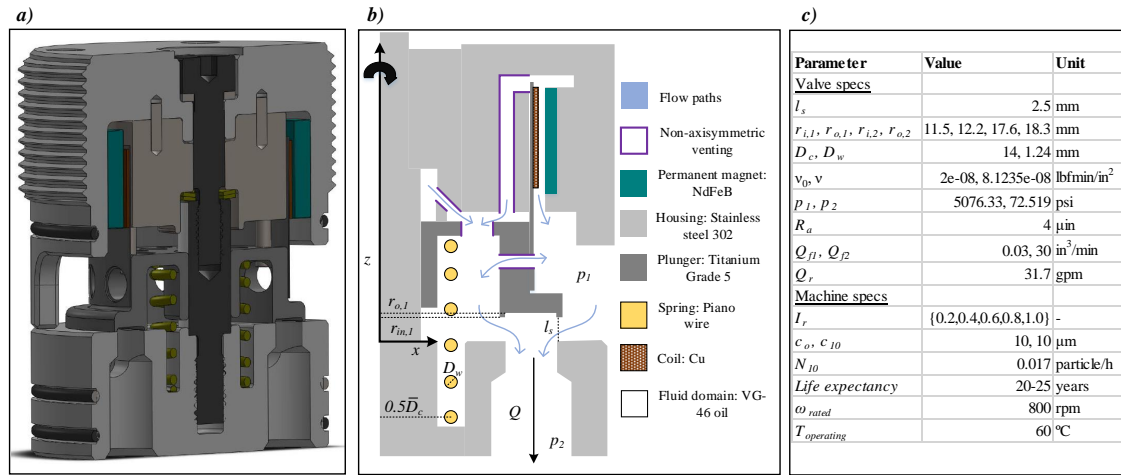
Figure 1: *a)* Cross-section view of the prototype FSV. *b)* Axisymmetric (*z*-axis) illustration of the FSV with appropriate notation and explanations. *c)* Numerical values of the parameters used in this paper.

and from this a reliability, $R \in (0, 1)$, may be derived from which the probability of system failure over time is calculated. However, this statistical based approach means that a failure often can not be traced back to the *physics of failure*, i.e. understanding the multi-disciplinary processes that result in the observed failure. For some engineering purposes it is sufficient to have an idea of a component's reliability throughout its life, but if it is desired to design a given system to withstand certain conditions a physics based approach must be applied.

3   FAULT TREE- & FAILURE MODE- ANALYSIS

A deductive failure analysis, or Fault Tree Analysis (**FTA**) has been performed on the FSV in order to understand how the system can fail. In this type of analysis, it is not the objective to clarify exactly at what rate and which physical phenomena cause the chain of events leading to failure. It is instead the objective to clarify these chain of events and theirs connection to one another. By this approach a FTA may be established as shown in Fig. 2.

The basic events described by A1-A8 contain all possible events that may contribute to progression of the failure it leads to, and is as such just an indication that something will be the cause of the different intermediate events, which ultimately cause the failure or degradation. For example A1 from Fig. 2 would include temperature of the coil, vibrations, over-current, contaminants etc. The FTA reveals that the FSV failure will occur if just one component fails, i.e. there does not exist any redundant components. An extension of the FTA is done to elaborate on the presumed dominating physical causes. The relevant failures of the FSV occur at: the contacting surfaces (Valve Seat Insert), the unidirectional cyclic spring and the moving coil actuator. The expected failure modes are elaborated as shown in Tab. 1 and explained in the subsections below.
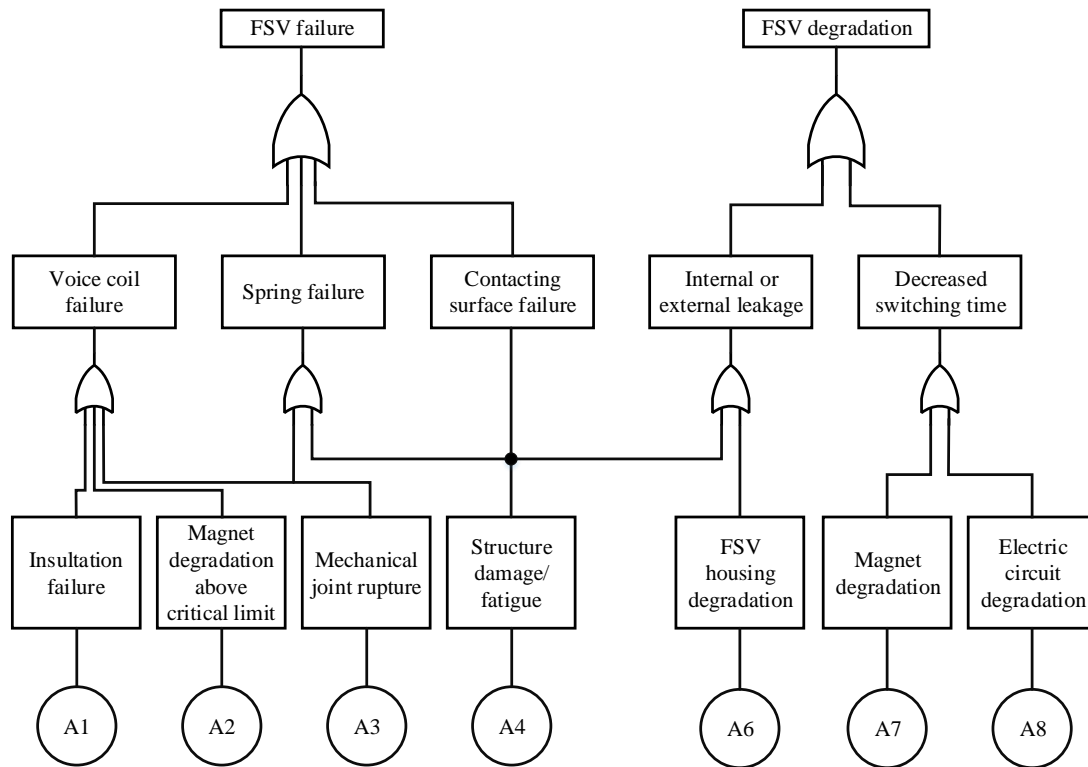
Figure 2: FTA in accordance to the fast switching valve. This FTA only considers the most relevant and obvious events.

Failure mode	Failure mechanism	Failure causes
Contacting surfaces (plunger & seat)		
Internal leakage	Worn plunger/seat	Repeated impact, differential pressure (fatigue), material flaws & contaminants
Stuck valve	Blockage or jammed plunger assembly	A sudden or gradual change in mechanical topology
	Sticking plunger	Invasive material at the sliding components
Unidirectional cyclic helical spring		
Valve always closed	Broken spring or damaged spring ends	Cyclic fatigue, corrosion & material flaws
Voice coil actuator		
Failure to close valve	Inoperative coil assembly	Overheated wire insulation, fatigue & sliding wear
	Permanent magnet demagnetization	Shock & thermal effects
	Decoupling of actuator & plunger	Shock & fatigue

Table 1: Failure mode analysis (major failure causes) with inspiration from [12]

3.1 Flow passages

A general analysis of flow passages in poppet valves is presented in [12] claiming the primary failure mode is wear caused by impact of contaminants, and that seating wear should be minimal if the design has correct seat material for the application. Furthermore, the following characteristics for reliability evaluation of a poppet type valve are suggested:

- Leakage tolerance

- Utilization rate

- Properties of the applied material(s) and fluid

- Fluid pressure

- Dimensions of the plunger/seat

- Surface roughness

- Fluid/material compatibility

- Corrosive environment

- Quality control/manufacturing processes

All the presented characteristics are in some sense quantifiable, although some are tedious to verify and difficult to translate into a universal framework to describe the physical degradation. Specifically, the state of environment and manufacturing process will in most cases involve an amount of uncertainty. Although most can be quantified, some may change over time and also the couplings between each characteristic may affect the reliability in non-linear or non-predictive ways, which then needs to be determined by experiments. All in all this makes a reliability analysis based on physics difficult, which is why the approach presented in section 4 is applied.

3.2 Mechanical springs

Mechanical springs are expected to operate over long periods of time without significant changes in dimension, displacement or spring rate. The lifetime of such springs dependent upon the susceptibility of the materials to corrosion and stress levels (static, cyclic or dynamic) [12]. Normal failure modes include fracture from fatigue and excessive loss of load from stress relaxation. By definition, a material that is loaded under oscillatory loads, fails when the stresses reach the materials fatigue limit. Conversely, a material that is loaded under static loads, fails when the stress reaches the materials yield limit, as explained in [12]. Normally the Soderberg failure criterion is used as a way of calculating the failure limit. Hereby a mixture of cyclic and static loads may be considered. The failure rate of a spring will typically be dependent on:

- Dimensions of the spring

- Properties of the applied material

- Level of loading

- Operating temperature

- Cyclic rate

- Corrosive environment

- Quality control/manufacturing processes

Although special cases may occur, making these characteristics difficult to quantify, it is expected that the reliability data from [12] can be extrapolated to the environment of a FSV due to similar loading conditions and equal applied spring material. Furthermore, the intended application is for very high performance, which is why the corrosiveness of the environment is expected to be limited.

3.3 Actuators

The primary topic of this paper concerns the mechanical topology. Therefore, the actuator failure rate is set to zero ($\lambda_{mc} = 0$). However, an analysis of the possible failure causes is presented to identify potential risks and these risks may then be quantified in further work.

The actuator used in the FSV is a moving coil surrounded by permanent magnets as may be observed from Fig. 1. The actuator is primarily used for closing of the valve, and when closed the pressure force ensures that the valve is kept closed. Therefore, overheating due to excessive power consumption is avoided and the risk of insulation failure is limited. The failure rate of an actuator as used in the FSV will be influenced by:

- Ohmic losses in the coil

- Properties of the applied material

- Power dissipation

- Operating temperature

- Operating frequency

- Vibrational shocks from the environment

- Corrosive environment

- Quality control/manufacturing processes

Consulting the FTA in Fig. 2, demagnetization of the magnet may be considered, which may be caused by either thermal effects (for NdFeB the Curie temperature is around 300°C [13]) or from vibrational shocks. A study of the flux degradation of NdFeB magnets at different temperatures over time shows that in a 30 year period no noticeable flux has been lost at 100°C [14]. The hydraulic oil is regulated to be around 60°C, but may locally be higher than 60°C around the coil when activated. This heat convection from ohmic losses in the copper coil has been analysed during the design phase and by using the known operating conditions the heat convection can be calculated. The steady state temperature stays below 100°C. The insulation used in the copper wire is designed to resist temperatures up to 200°C. However, the surrounding oil and possible contaminants

may also result in insulation failure. If debris enter the gap between the moving coil and magnet abrasive wear may cause a failure. The wire connection supplying the moving coil is expected to be a location with risk of long term fatigue because of the wire bending when the plunger is displaced. The presented analysis shows that some design considerations have been taken to limit the risk of failure, but that the probability of the presented events occurring is unknown.

4   FAILURE RATES

The reliability of any component R_i may be described by its failure rate during some time frame, the higher the reliability the lower the risk of failure. The rate may be applied in Eq. (1) along with a time (t) dimension corresponding to the given failure rate, e.g. failures per million hours leads to t having the unit million hours.

$$R_i = e^{-\lambda_i t} \tag{1}$$

The total reliability (R_{tot}) is directly based on each components reliability, and its influence on the specific failure. Thus, if several components need to fail in order for a failure to occur, R is the first case of Eq. (2). Correspondingly R may be described by the second case if only one component needs to fail for a failure to arise.

$$R_{tot} = \begin{cases} 1 - \prod_{i=1}^{n}(1 - R_i) & \text{if } \delta_1 = 0 \text{ and } \delta_2 = 0 \rightarrow \delta_{tot} = 0 \\ \prod_{i=1}^{n} R_i & \text{if } \delta_1 = 0 \text{ or } \delta_2 = 0 \rightarrow \delta_{tot} = 0 \end{cases} \tag{2}$$

Here δ is a discrete parameter that can take the value 1 if the component is working as intended and 0 if it has failed. This may be used to express the total reliability as:

$$R_{tot} = R_{cs}R_{hs}R_{mc} = e^{-(\lambda_{cs} + \lambda_{hs} + \lambda_{mc})t} \tag{3}$$

The indexes denote Contacting Surfaces (cs), Helical Spring (hs) and Moving Coil (mc).

4.1   Contacting surface failure rate

The mechanical topology governing the flow characteristic of the FSV is expected to degrade over time due to repeated loadings, erosion from moving fluid with potential contaminants and/or by other environmental corrosion. A general approach to determine the failure rate of this in a poppet valve has been found in [12], and is given as:

$$\lambda_{cs} = \lambda_{cs,b}C_pC_QC_fC_VC_cC_\sigma C_{D_s}C_{L_w}C_w \tag{4}$$

The coefficients (C_i) have been determined by empirical data. It should in this regard be noted that the tests were conducted around 30 years ago, hence not accounting for modern manufacturing techniques with material hardening and surface coatings. The failure rate is thus expected to be a very conservative fit based on experience for other valves. The source [12] is American, why also the used units are American. This mix of notation is maintained here to avoid any misconceptions. The failure rate coefficients are functions of different parameters, as visualized in [12] and are therefore not done here. The test data for a poppet type seat is interpolated to yield the following coefficients:

$C_p = \left(\frac{p_1-p_2}{3000}\right)^2$	considers the fluid pressure differential
$C_Q = 4.2 - 79Q_f$	considers the amount of allowable leakage when $Q_f \leq 0.03$ in^3/min
$C_Q = \frac{0.055}{Q_f}$	considers the amount of allowable leakage when $Q_f > 0.03$ in^3/min
$C_f = \frac{R_a^{1.65}}{353}$	considers the surface finish of contacting material
$C_v = \frac{v_0}{v}$	considers the fluid viscosity at a given operating temperature
$C_c = \left(\frac{c_o}{c_{10}}\right)^3 Q_r N_{10}$	considers the effect of contaminants
$C_\sigma = 0.26 \left(\frac{9000}{\sigma_s}\right)^{1.5}$	considers the contact pressure required to avoid leakage, where
$\sigma_s = \frac{\Delta p(r_{o,2}^2 - r_{in,1}^2)}{(r_{o,1}^2 - r_{in,1}^2 + r_{o,2}^2 - r_{in,2}^2)}$	
$C_{D_s} = 1.1D_s + 0.32$	considers the seat diameter, where
$D_s = 2(r_{in,2} - r_{in,1})$	in
$C_{L_w} = 3.55 - 24.52L_w + 72.99L_w^2 - 85.75L_w^3$	considers the land width of the seat and plunger when $L_w \leq 0.34$, where
$L_w = r_{o,1} - r_{in,1} + r_{o,2} - r_{in,2}$	in
$C_{L_w} = 0.25$	considers the land width of the seat and plunger when $L_w > 0.34$ in
$C_w = 1 + F_l^2$	considers the rated flow rate

Where c_{10} is the standard system filter size, c_o is the used system filter size, R_a is the surface finish (Arithmetical mean roughness), N_{10} is the number of steel particles under 10 micron generated per hour at rated flow, Q_r is the rated flow, Q_f is the allowable leakage, σ_s is the surface contact pressure, $\Delta p = p_1 - p_2$ is the pressure differential, λ_{cs} is the failure rate of the contacting surfaces at some base failure rate ($\lambda_{cs,b} = 1.4$ failures per million operations). The soft parameters here constitute: R_a, c_o, N_{10}, the values of these have been determined based on [12] in order to illustrate the design sensitivity to the different parameters. The number of steel particles per hour is taken for a piston pump, the surface finish for high performance systems can be expected in the range 1-4μin and to be conservative it is decided to use 4μin. The filter size is defined to be of standard size at 10μm.

The failure rate coefficients are shown in Fig. 3 and the same coefficients normalized are presented in Fig. 4. The applied design parameters and the corresponding failure rate coefficient involves uncertainty. Therefore, a $\pm 20\%$ sensitivity interval is illustrated with red in both figures. This procedure is done by evaluating the failure rate coefficients with a change of each governing parameter by the prescribed range, e.g. C_c is governed by: c_o, Q_r, N_{10}, where an increase of any of these would correspond to an increase in failure rate. This coefficient can therefore potentially be affected by three uncertainties and one non-linearity (following the expression) thus the range of uncertainty depends upon the initial value of filter size (c_0).

Each coefficient of Fig. 3 affects the combined failure rate in a linear manner where coefficients above 1 contribute to shorter lifetime and below the opposite. From this consideration three coefficients limit the lifetime, C_p, C_Q & C_{L_w}. One leaves it unchanged
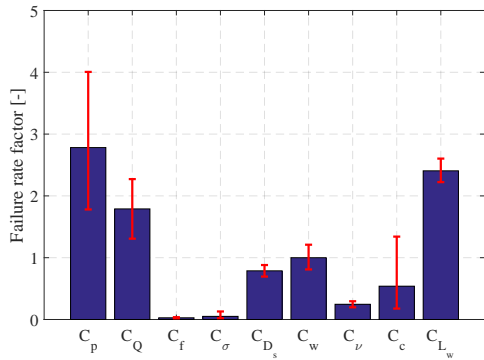
Figure 3: Distribution of the different flow passage failure rate (λ_{cs}) coefficients.
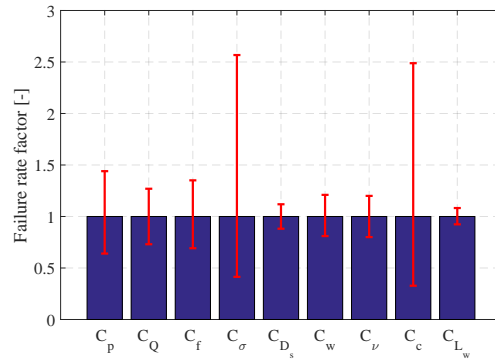
Figure 4: Normalized failure rate coefficients of the flow passage.

and the rest extends the lifetime. The pressure differential along with the width of the contacting surfaces contribute to a significant increase in risk of failure. Among these the land width is a geometrical property that can be redesigned, though at the cost of larger stiction forces when opening the FSV resulting in energy loss. Furthermore, the data says that any changes above a 0.34in (8.64mm) land width makes no difference in reliability. The pressure differential is governed by the overall system in which the FSV is applied, as is the amount and size of contaminants. In fact it is seen that the non-linear term of C_c causes the filter size to have a significant influence on the failure rate and the sensitivity of this coefficient is very high relative to the other coefficients. The only coefficient that match this range of uncertainty is the contact pressure coefficient (C_σ) that also show a non-linear tendency. The final failure rate is therefore very sensitive to these, thus to pursue enhancements towards longer lifetimes of the valves, these parameters are relevant to consider.

The topology used in [12] is a poppet as presented in Fig. 5 and the outlet is shaped as a circular pipe and not an annulus, as is the case in the FSV shown to the right. This influences C_σ which constitute a large margin of uncertainty, the difference is therefore highlighted.
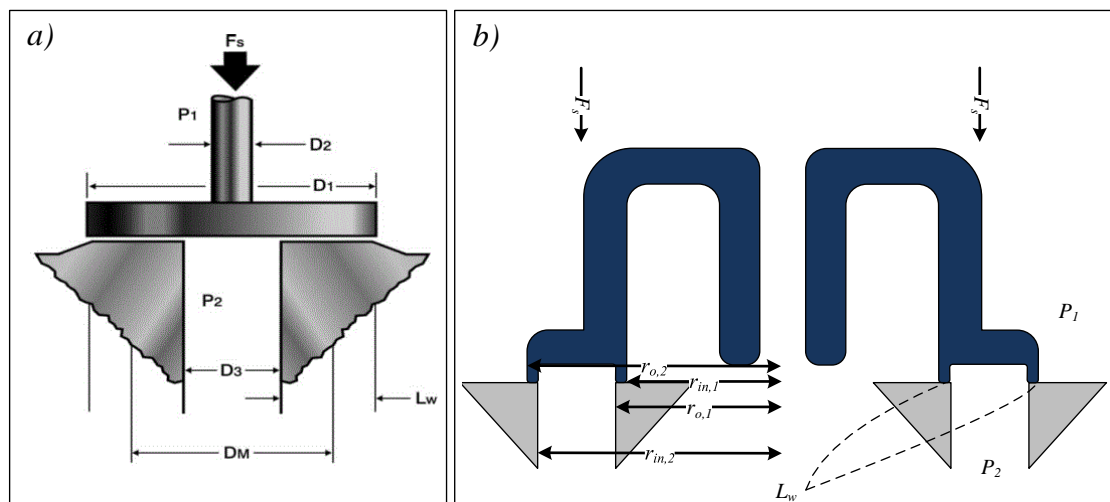
Figure 5: Difference between the mechanical topology of *a)* the poppet valve design from [12] and *b)* the FSV prototype.

The seat pressure in the FSV is affected by a different area ratio described as:

$$\sigma_s = \underbrace{\frac{\Delta p(r_1^2 - r_2^2)}{r_1^2 - r_3^2}}_{circular} \quad \text{transformed} \quad \text{to} \quad \sigma_s = \underbrace{\frac{\Delta p(r_{o,2}^2 - r_{in,1}^2)}{(r_{o,1}^2 - r_{in,1}^2 + r_{o,2}^2 - r_{in,2}^2)}}_{annulus} \tag{5}$$

This discrepancy shows that several radii affect the contact pressure and the sensitivity of the design thus depend on one additional geometric parameter. However, the fundamental idea behind the contact pressure is maintained and thus expected to be a valid reformulation.

In total the estimated failure rate includes a level of uncertainty caused by the difference in topology and sizes that can have a certain uncertainty. However, this analysis does give a rough guideline about where an issue may occur, and more importantly to illustrate the significance of the different factors influencing the lifetime with potential non-linear effects.

4.2 Unidirectional helical cyclic spring failure rate

The spring used in the FSV is pre-compressed (31 N) and will not experience tension. The number of turns in the spring is 5 and with the pre-compression, there is a distance of 3.5 mm between each turn. Therefore, it is expected that all turns will always be active. It is therefore unidirectional and the topology is helical, which from [12] translates to the following failure rate:

$$\lambda_{hs} = \lambda_{hs,b} C_g C_{D_w} C_{D_c} C_{N_a} C_y C_l C_k C_{N_m} C_r C_m \tag{6}$$

where for a helical spring made of piano wire:

$C_g = \left(\frac{G_m}{11.5}\right)^3$ considers the rigidity of the spring material

$C_{D_w} = \left(\frac{D_w}{0.085}\right)^3$ considers the wire diameter of the spring

$C_{D_c} = \left(\frac{0.58}{\overline{D}_c}\right)^6$ considers the mean coil diameter of the spring

$C_{N_a} = \left(\frac{14}{N_a}\right)^3$ considers the number of active turns of the spring

$C_y = \left(\frac{0.19}{T_s}\right)^3$ considers the tensile strength of the spring material

$C_l = \left(\frac{l_s}{1.07}\right)^3$ considers the maximum deflection of the spring

$C_k = \left(\frac{K_w}{1.219}\right)^3$ considers the spring concentration factor (K_w)

where $K_w = \frac{4r-1}{4r-4} + \frac{0.615}{r} \quad ; \quad r = \frac{\overline{D}_c}{D_w}$

$C_{N_m} = \left(\frac{N_m}{300}\right)^3$ considers the number of operating cycles per minute

$N_m = \omega_{rated} I_r$

$C_r = 1$ considers the effect of a corrosive environment, 1 if no effect

$C_m = 1$ considers malformations from the manufacturing process, 1 if no effect thus identical springs

Here D_w is the wire diameter, $\overline{D}_c$ is the mean coil diameter, G_m is the modulus of rigidity (10 Mlbs/in^2), N_a is the number of active turns (5), N_m is the spring cycle rate, T_s

is the tensile strength of the spring material (0.227 Mlbs/in^2), λ_{hs} is the spring failure rate at some base failure rate ($\lambda_{hs,b} = 23.8$ failures per million hours).

The failure rate coefficients are shown in Fig. 6 and the same coefficients normalized are presented in Fig. 7.
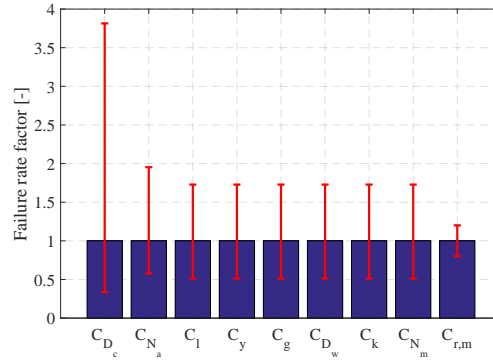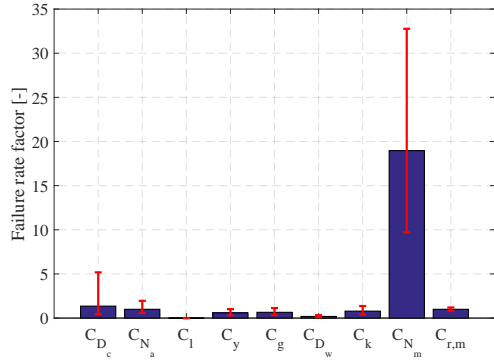
Figure 6: Distribution of the different helical spring failure rate (λ_{hs}) coefficients.

Figure 7: Normalized failure rate coefficients of the helical spring.

The designs sensitivity to the coefficients describing the spring lifetime are identical in almost all of the cases. However, the mean diameter of the spring can potentially result in a massive change of lifetime if this diameter drops well below 0.58in (14.73mm). The fraction describing this is raised to the power of six and is thus not surprisingly very sensitive to changes. Many of the spring dimensions are well known, and production tolerances are low meaning the presented values are representative for the applied spring.

5 VISUALIZATION OF THE FAILURE RATES

The failure rates are converted into a common time frame, namely failures/million hours. This allows combination of the failure rates for the flow passage and spring. Furthermore, it is relevant to consider different ratios of idle operations during the valves life. This ratio is defined as:

$$I_r = 1 - \gamma \tag{7}$$

where γ is the fraction of idling cycles and $\gamma = \begin{bmatrix} 0 & 0.2 & 0.4 & 0.6 & 0.8 \end{bmatrix}$ is analysed. The reliability of the flow passage at low and high leakage level is shown in Fig. 8 where the dotted black line is used to illustrate the total reliability, i.e. the influence of spring reliability is included.

It is observed from Fig. 8 that the reliability of the flow passage reaches a high risk of failure before 5 years of operation regardless of the idle range. Compared to the demanded lifetime around 20 years this is therefore a reason for concern. However, the leakage level is low during this failure and not critical. By allowing 0.5 L/min, which is still well below the rated flow results in a leakage failure probability of 10% over a 25 year period. Although this probability is only a rough estimate it is a promising result. It is therefore relevant to investigate the amount of leakage which is allowed before the machine feasibility is compromised, this is left for further studies. In a similar fashion, the spring reliability has a visual influence on the total reliability and under maximum load conditions the spring reliability can not necessarily be discarded.
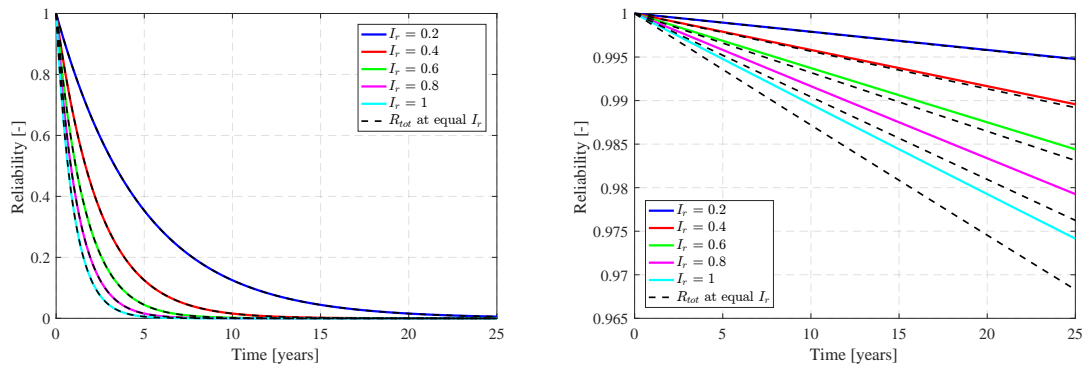
Figure 8: Distribution of the reliability of only the flow passage (coloured lines) compared with the total reliability with multiplication of the spring reliability (dashed lines). **Left:** Probability of failure indicating a maximum acceptable leakage of $Q_{f1} = 0.0005$ L/min. **Right:** Probability of failure indicating a maximum acceptable leakage of $Q_{f2} = 0.5$ L/min.

6 STRUCTURAL ANALYSIS OF THE CONTACTING SURFACES

The possibility of failure in the valve seat may by investigated by calculating the stress that will develop during operation of the FSV. Especially, the contacting surfaces are of interest and here the focus is directed to the maximum principal stresses due to theirs documented importance in fatigue analysis [15]. The analysis is done by FEA in ANSYS workbench 18 with appropriate settings for contact problems. The interaction between contacting bodies and surfaces must be defined a priori of the analysis, and to emphasize the importance of this; *bonded* (no tangential or normal traction allowed), *rough* (no tangential but with normal traction allowed) & *frictionless* (both tangential and normal traction allowed) are analysed. This is done to clarify the span of uncertainty correlated to FEA when dealing with contact problems. Furthermore, the mesh quality in structural problems must not be too coarse nor too fine, and the so called *sweet-spot* has been pursued iteratively to show fast convergence with realistic stresses. A total of 1.8e6 elements and 3e6 nodes are used with an inflation layer near the contacting surface with height 25μm and a refinement on the surface of contact. This is shown in the result figures below.

The software can apply different algorithms to define the contact boundary conditions, an *Augmented Lagrangian* contact formulation is used in this analysis since it allows computation of both the contact- (plunger) and target- (seat) body stresses. The main drawback of this type of formulation is that it allows small virtual penetration of the two bodies and a normal contact stiffness is therefore used to compute a counteracting force. The value of this can either be pre-defined or program controlled where it is updated iteratively to fit the specific contact problem - the latter option is used. This formulation uses integration point detection, resulting in more detection points than if the nodal detection from *Normal Lagrange* or *Multi-Point Constraint* is used. This allows a coarser mesh in the contact region and is beneficial to reduce the computational time and maintaining good accuracy.

The pressure used for the structural analysis is defined as $p_1 - p_2$ from Fig. 5 and it is decided to maintain the simplicity of the analysis by considering a constant pressure difference of 349 bar. This may in further work be extended to consider possible adhesive forces caused by separation of surfaces along with impact forces. The calculated max-

imum principal stresses in the plunger and seat are shown in Fig. 9 where the critical zones on plunger and seat are visualized. The contact pressure between plunger and seat for two different formulations are presented in Fig. 10 & 11. The contacting surfaces penetrate at worst case with 2.8e-3, 0.2 & 0.1μm for the *bonded*, *rough* and *frictionless* case respectively. This is an indication that the results of the *bonded* analysis represents real conditions most accurately since the two bodies will not penetrate in reality.
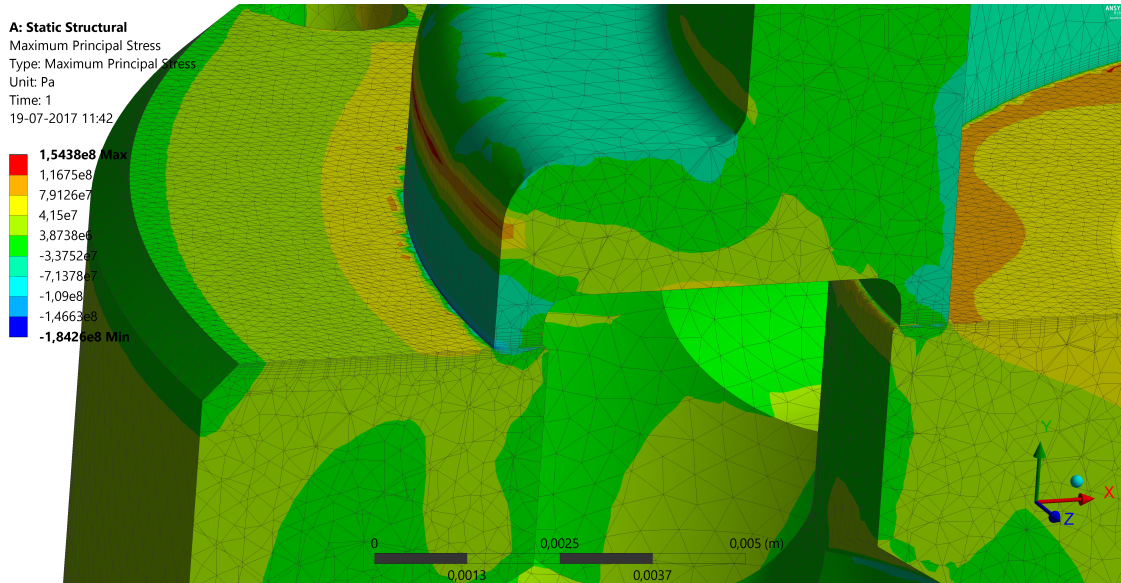
Figure 9: FEA of the maximum principal stress from a *frictionless* structural analysis of the flow geometry when $\Delta p = 349$ bar. The stress concentration on the outer ring of the plunger contains the point with maximum stress (Cr_p).
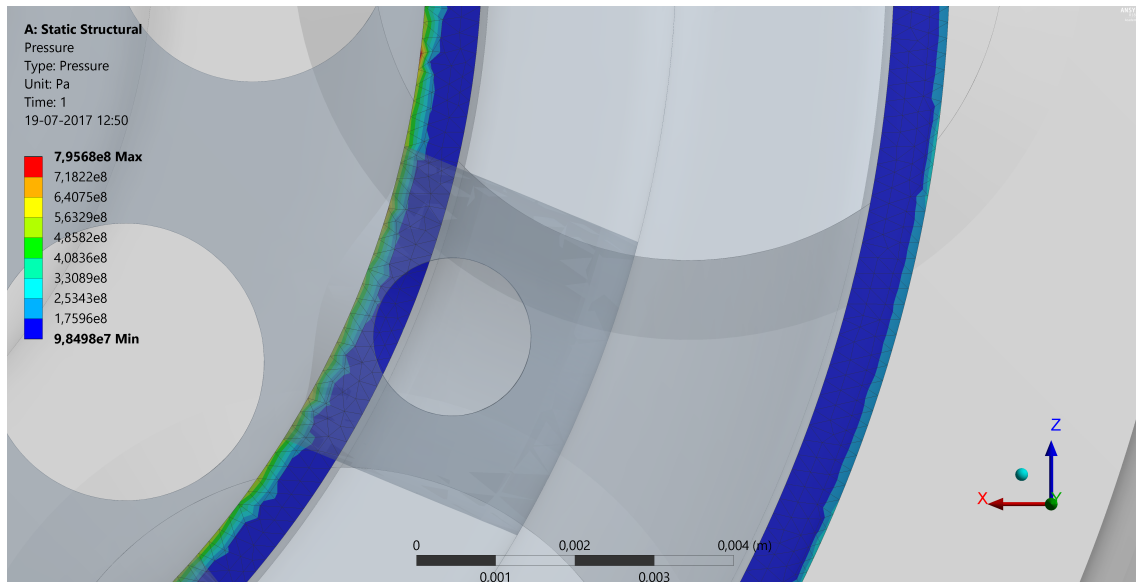
Figure 10: Sample of the *bonded* contact pressure.

The pressure distributions reveals inconsistency between maximum pressure occurring in the inner annulus or outer annulus. The *bonded* contact gives rise to a sharp pressure increase at $r_{in,1}$, on the contrary the *frictionless* analysis yield a more smooth
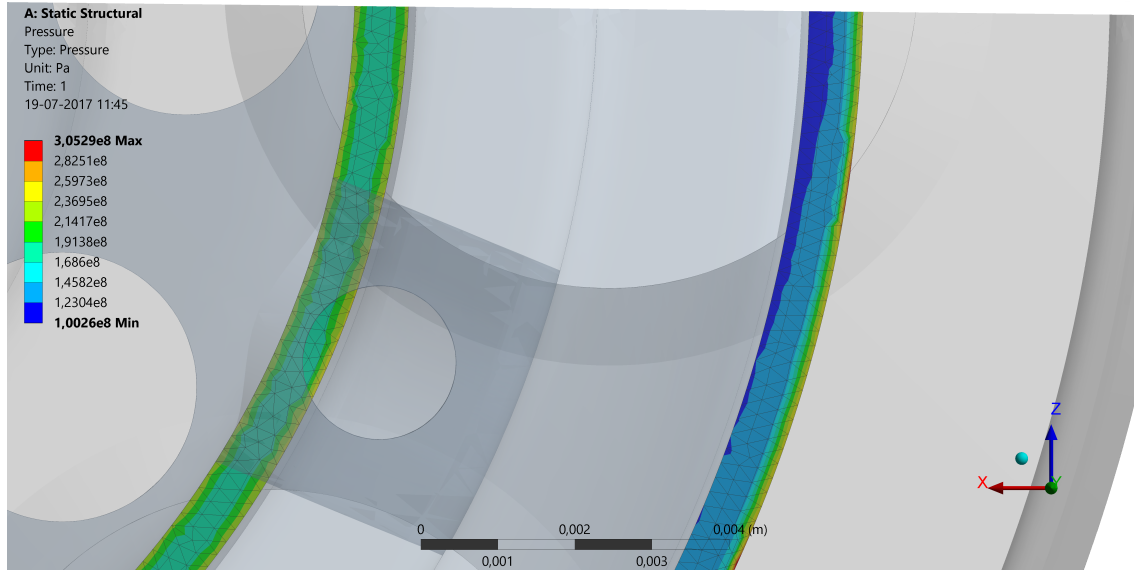
Figure 11: Sample of the *frictionless* contact pressure.

distribution of the pressure. However, it now increases at $r_{o,2}$, i.e. the difference in contact penetration and the fact that tangential and normal traction is allowed results in a less stiff system with the possibility of smoothing the load. None of the solutions can be concluded more accurate than the other, but the range of the results does give an indication of the material stress conditions.

The fatigue of the Valve Seat Insert (**VSI**) is estimated by using the principal stresses combined with the material fatigue endurance limit (σ_e). The actual endurance limit will depend on several parameters such as the type of loads, initial flaw sizes, surface roughness, temperatures and a reliability factor. The type of load is expected to have a relationship between maximum and minimum stress of $R = 0$, i.e. the material is loaded and then unloaded each cycle. This type of loading profile is associated with long life time, and from a Goodman relationship the corrected endurance limit may approximated by [16]:

$$\sigma_e' = \sigma_e \left(1 - \frac{\sigma_m}{\sigma_u} \right) \tag{8}$$

where the mean and ultimate yield stress (σ_m, σ_u) are used to scale the endurance limit. This factor will be in the range of 0.8-0.9 and to ensure a conservative design the maximum stresses should be kept well below this limit. The distribution of principal stresses near the VSI are shown in Fig. 9. The computed stress levels are given in Tab. 2, which shows a contact pressure in the range of 300-800 MPa at either the inner contact radius or the outer contact radius from Fig. 5. The occurrence of maximum principal stresses depends upon the formulation and here the *bonded* contact involves the most critical level, however, still around a factor two below the endurance limit. Material fatigue is therefore no major concern from a static analysis.

There are shortcomings to the presented FEA when describing the interaction of the two bodies (assumed smooth surfaces, no impact stress and no adhesive forces from unloading). The combination of conversion of kinetic energy (in the plunger) to internal energy (in the seat) and the interaction of a hydraulic fluid will give rise to additional considerations. An analysis of such problem is presented in [19] where two tori are brought into contact and a piezo-viscous model is used to evaluate the squeeze film pressure. The

Parameter	Bonded contact		Rough contact		Frictionless contact		unit
	Plunger	*Seat*	*Plunger*	*Seat*	*Plunger*	*Seat*	
$\sigma_{princ,max}$	93 at Cr_p	219 at $r_{o,2}$	183 at Cr_p	56 at $r_{in,1}$	154 at Cr_p	120 at $r_{in,1}$	[MPa]
$p_{c,max}$	795 at $r_{in,1}$	795 at $r_{in,1}$	543 at $r_{in,1}$	543 at $r_{in,1}$	300 at $r_{o,2}$	300 at $r_{o,2}$	[MPa]
			Material parameters		Ti6Al4V [17]	Impax supreme [18]	
E	-	-	-	-	105	200	[GPa]
v	-	-	-	-	0.36	0.3	[-]
ρ	-	-	-	-	4430	7800	[kg/m^3]
σ_e/σ_u	-	-	-	-	510/1070	400/1000	[MPa]

Table 2: Results from static FEA and applied material parameters. Simulation periods: *bonded*: 24 min, *rough*: 90 min, *frictionless*: 66 min.

results show that the fluid pressure locally exceeds the Hertzian contact pressure at impact, and the consequence of this is interesting as a further study.

6.1 Lumped model based on Hertz theory

The reason for applying a numerical method is due to the complexity of solving the contact problem analytically, and the locations of critical stresses are not feasible to determine analytically for this topology. However, an approximation of the contact pressure can be found by Hertz theory. This is done by assuming the contact to be similar to that of two elastic tori, which again is similar to that of two elastic cylinders of length, $L_i = 2\pi R_i$. This solution is computationally efficient and interesting to compare with the different numerical contact formulations. It is evaluated by:

$$p_i(x_i) = p_{0,i} \left(1 - \frac{x_i^2}{a_i^2} \right)^{1/2} \tag{9}$$

where a is the half-width of the contact area by Eq. (10), p_0 is the maximum pressure given by Eq. (11) and x is the spatial coordinate on the x-axis where $x = 0$ at the center of contact [20].

$$a_i = \left(\frac{4F_{n,i}\overline{r}_i}{L_i \pi \overline{E}} \right)^{1/2} = \left(\frac{2F_{n,i}\overline{r}_i}{R_i \pi^2 \overline{E}} \right)^{1/2} \tag{10}$$

$$p_{0,i} = \left(\frac{F_{n,i}\overline{E}}{2\pi^2 R_i \overline{r}_i} \right)^{1/2} \tag{11}$$

The contact area and maximum pressure is thus described by geometric and material specific properties combined with some normal load applied to the contacting bodies. These relations are defined as:

$$\frac{1}{\overline{r}_i} = \frac{2}{r_i} \quad ; \quad \frac{1}{\overline{E}} = \frac{1-v_1^2}{E_1} + \frac{1-v_2^2}{E_2}$$

$$R_i = \frac{r_{in,i}+r_{o,i}}{2} \quad ; \quad r_i = \alpha R_i \quad ; \quad r_m = \frac{r_{o,2}+r_{o,1}}{2}$$

$$F_{n,1} = \pi \left(p_1(r_m^2 - r_{o,1}^2) - p_2(r_m^2 - r_{in,1}^2) \right) \quad ; \quad F_{n,2} = \pi \left(p_1(r_{o,2}^2 - r_m^2) - p_2(r_{in,2}^2 - r_m^2) \right)$$

where E is Young's modulus of elasticity for the respective material, v is Poisson's ratio for the respective material, α is the aspect ratio of 0.1 to neglect curvature from the major radii (R_1 & R_2), r is the minor radius of the torus and F_n is the estimated normal force. The geometrical parameters can be observed in Fig. 12 and the corresponding Hertz pressure is shown in Fig. 13. The width of the contact area is a factor of 10 smaller than for the FSV (0.08 vs 0.7mm). The difference in contact area between the tori approximation and the FSV will definitely cause Hertz pressure peaks to be above the ones expected in reality. This is also what is observed when compared with the FEA results in Tab. 2, where the Hertz peak pressure of 2.3GPa in the inner torus is 3-5 times larger than the peak from FEA. It is concluded that the presented lumped model using a Hertz approach involves uncertainty.
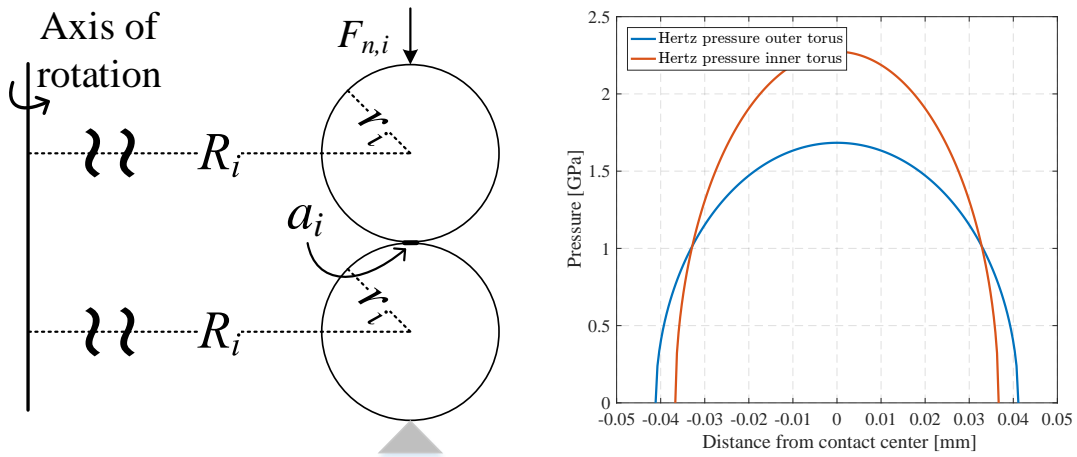
Figure 12: Simplified contact geometry.

Figure 13: Pressure distributions by Hertz theory.

7 CONCLUSION AND FURTHER WORK

In this paper a statistical based reliability model has been applied on a hydraulic fast switching valve. This is supported by a reliability analysis of the system including a fault tree analysis and analysis of the different obvious failure modes. The analysis shows no redundancies in the design and outlays the actual complexity in predicting the lifetime of the FSV.

The failure rate of the flow geometry depends upon the definition of a critical internal leakage rate. A study of what is considered a low leakage (0.0005 L/min) and a high leakage (0.5 L/min) when compared to nominal valve flow rates was presented. This was used to illustrate the change in system reliability when a larger tolerance is allowed to aid in understanding the sensitivity of this type of analysis. Furthermore, a $\pm 20\%$ sensitivity analysis of each failure rate coefficient was plotted showing which system parameters may be relevant to consider when making a durable mechanical topology as used in FSVs. Especially contact pressure and contaminated oil were shown to scale in a non-linear manner, where the debris particle sizes and amount could affect the failure rate significantly.

The concern about possible failure in the flow geometry lead to a structural analysis of the maximum principal stresses developing in the valve seat. This was done for the

plunger and seat contact with a load condition corresponding to maximum fluid pressure occurring in a DD machine. These loads were calculated from *bonded*, *rough* and *frictionless* contact showing equal magnitude of stress within a range sufficiently below the endurance limit of the applied materials. Different critical zones were identified with regards to the used formulation, emphasizing the complexity of accurately simulating the contact stresses. The resulting contact pressures also vary w.r.t. contact formulation and when compared to a simplified Hertz calculation large discrepancies were observed. In conclusion the VSI is not at high risk of fatigue, instead the design is susceptible to wear related phenomena which may lead to failure. A study of the significance from impact, surface roughness, mixed-lubrication and material removal is therefore highly relevant to study this failure mode further.

ACKNOWLEDGEMENT

References

[1] G. S. Payne, U. B. P. Stein, M. Ehsan, N. J. Caldwell, and W. H. S. Rampen, "Potential of Digital Displacement Hydraulics for Wave Energy Conversion," *6th European Wave and Tidal Energy Conference*, 2005.

[2] B. Winkler and R. Scheidl, "Development of a fast seat type switching valve for big flow rates," *The Tenth Scandinavian International Conference on Fluid Power*, pp. 137–146, 2007.

[3] A. Ploeckinger, B. Winkler, and R. Scheidl, "Development and prototyping of a compact, fast 3/2 way switching valve with integrated onboard electronics.," *Proceedings of the 11th Scandinavian International Conference on Fluid Power*, 2009.

[4] B. Winkler, A. Ploeckinger, and R. Scheidl, "A novel piloted fast switching multi poppet valve," *International Journal of Fluid Power*, vol. 11, no. 3, pp. 7–14, 2010.

[5] J. P. Uusitalo, V. Ahola, L. Soederlund, M. Linjama, and L. Kettunen, "Novel Bistable Hammer Valve For Digital Hydraulics," *International Journal of Fluid Power*, vol. 11, no. 3, pp. 35–44, 2010.

[6] D. B. Roemer, *Design and Optimization of Fast Switching Valves for Large Scale Digital Hydraulic Motors*. PhD thesis, Department of Energy Technology, The Faculty of Engineering and Science, Aalborg University, 2014.

[7] M. Paloniitty, L. Matti, and K. Huhtala, "Durability Study on High Speed Water Hydraulic Minitaure on/off Valve," in *The Fifth Workshop on Digital Fluid Power*, (Tampere, Finland), pp. 201–212, 2016.

[8] H. C. Meng and K. C. Ludema, "Wear models and predictive equations: their form and content," *Wear*, vol. 181, pp. 443–457, 1995.

[9] J. A. Williams, "Wear and wear particles - some fundamentals," *Tribology International*, vol. 38, no. 10, pp. 863–870, 2005.

[10] C. Noergaard, M. M. Beck, D. B. Roemer, and H. C. Pedersen, "OPTIMIZATION OF MOVING COIL ACTUATORS FOR DIGITAL DISPLACEMENT MACHINES," in *The Eighth Workshop on Digital Fluid Power*, (Tampere, Finland), 2016.

[11] G. A. Klutke, P. C. Kiessler, and M. A. Wortman, "A Critical Look at the Bathtub Curve," *IEEE transactions on reliability*, vol. 52, no. 1, pp. 125–129, 2003.

[12] D. C. Naval Surface Warfare Center, *Handbook of reliability prediction procedures for mechanical equipment*. No. May, 2011.

[13] S. H. Kim and C. Doose, "Temperature compensation of NdFeB permanent magnets," *Proceedings of the 1997 Particle Accelerator Conference*, vol. 3, pp. 3227–3229, 1997.

[14] M. Haavisto and M. Paju, "Time-Dependent Demagnetization in Sintered NdFeB Magnets," in *Proceedings of the 21st Workshop on Rare-Earth Permanent Magnets and their Applications*, pp. 224–226.

[15] L. Witek, "Failure and thermo-mechanical stress analysis of the exhaust valve of diesel engine," *Engineering Failure Analysis*, vol. 66, pp. 154–165, 2016.

[16] S. Oller, O. Salomon, and E. Onate, "A continuum mechanics model for mechanical fatigue analysis," *Computational Material Science*, vol. 32, no. 2, pp. 175–195, 2004.

[17] R. Boyer, G. Welsch, and E. W. Collings, *No Materials Properties Handbook: Titanium Alloys*. 1994.

[18] K. Karlén and M. Olsson, "An investigation of the location of fatigue initiation - Deterministic and probabilistic aspects," *International Journal of Fatigue*, vol. 66, pp. 65–77, 2014.

[19] P. Johansen, N. C. Bender, A. H. Hansen, and L. Schmidt, "Investigation of squeeze film damping and associated loads," in *Fluid Power & Motion Control*, 2017.

[20] K. L. Johnson, *Contact Mechanics*. Cambridge University Press, 1985.